

Di-nucleon structures in homogeneous nuclear matter based on two- and three-nucleon interactions

Hugo F. Arellano^{1,2}, Felipe Isaule¹, and Arnau Rios³

¹ Department of Physics - FCFM, University of Chile, Av. Blanco Encalada 2008, Santiago, Chile

² CEA, DAM, DIF, F-91297 Arpajon, France

³ Department of Physics, Faculty of Engineering and Physical Sciences, University of Surrey, Guildford, Surrey GU2 7XH, United Kingdom

Received: date / Revised version: date

Abstract. We investigate homogeneous nuclear matter within the Brueckner-Hartree-Fock (BHF) approach in the limits of isospin-symmetric nuclear matter (SNM) as well as pure neutron matter at zero temperature. The study is based on realistic representations of the internucleon interaction as given by Argonne v18, Paris, Nijmegen I and II potentials, in addition to chiral N³LO interactions, including three-nucleon forces up to N²LO. Particular attention is paid to the presence of di-nucleon bound state structures in ¹S₀ and ³SD₁ channels, whose explicit account becomes crucial for the stability of self-consistent solutions at low densities. A characterization of these solutions and associated bound states is discussed. We confirm that coexisting BHF single-particle solutions in SNM, at Fermi momenta in the range 0.13 – 0.3 fm⁻¹, is a robust feature under the choice of realistic internucleon potentials.

PACS. 21.65.-f Nuclear matter – 21.45.Bc Two-nucleon system – 21.65.Mn Equations of state of nuclear matter

1 Introduction

One of the main goals in theoretical nuclear physics is that of accounting for nuclear structures and processes starting from the basic interaction among their constituents. If sub-hadronic degrees of freedom (i.e. quarks and gluons) are not treated explicitly, then this goal relies on realistic representation of the bare internucleon interaction. Such is the case of modern interactions based on quantum-field models, where strengths and form factors are adjusted to best reproduce nucleon-nucleon (*NN*) scattering observables as well as properties of the deuteron, the only *NN* bound state in free space. The inclusion of three-nucleon (*3N*) forces become subject to constraints from three-body bound state data and/or homogeneous nuclear matter [1, 2].

Homogeneous nuclear matter, a hypothetical infinite medium of neutrons and protons, is among the simplest many-body nuclear systems. In principle, all properties of this system should be inferred from the bare interaction among its constituents. In this context the Brueckner-Hartree-Fock (BHF) non-relativistic approach at zero temperature offers a well defined framework which enables the evaluation of the energy of the system as a function of the nucleon density $\rho = \rho_p + \rho_n$, and isospin asymmetry $\beta = (\rho_n - \rho_p)/(\rho_n + \rho_p)$, with ρ_p (ρ_n) denoting proton (neutron) density [1, 3]. Extensive applications of the BHF

approach has served to assess the consistency of the model to account for saturation properties of isospin-symmetric ($\beta = 0$) nuclear matter [1, 4, 5]. Not only that but also the resulting BHF *g* matrix at positive energies has served as an important tool to construct *NN* effective interactions, subsequently used in the evaluation of microscopic optical model potentials for nucleon scattering off finite nuclei [6].

In this work we investigate homogeneous nuclear matter in the framework of the BHF approach at zero temperature considering realistic representations of the bare *NN* interactions. Particular attention is paid to the manifestation of two-nucleon bound state structures (di-nucleons), expressed as singularities in the *g* matrix in the search process for self-consistent solutions of single-particle (sp) spectra. As such, this work represents an extension of the investigation reported in Ref. [7] based on Argonne *v*₁₈ (AV18) [8], where an explicit account for di-nucleon structures in symmetric nuclear matter was first reported. Among the main findings reported in that work we mention: *a*) Nucleon effective masses at low densities can reach up to four times the bare nucleon mass; *b*) Large size di-nucleon bound states take place at sub-saturation densities; and *c*) Coexisting sp spectra are identified at low densities, that is to say two distinct sp fields meet self-consistency at a same density. Here we investigate the robustness of these features in SNM under the choice of the bare *NN* interaction, in addition to their manifestation in the extreme case of pure neutron matter.

Send offprint requests to:

The BHF approach for interacting nucleons in nuclear matter can be thought as the lowest-order approximation of Brueckner-Bethe-Goldstone (BBG) theory or Self-Consistent Green's Function theory at zero temperature [3]. The former is based on the hole-line expansion for the ground state energy [1], where Goldstone diagrams are grouped according to their number of hole lines, with each group summed up separately. The BHF approximation results from the summation of the two-hole-line diagrams, with the *in-medium* two-body scattering matrix calculated self-consistently with the sp energy spectrum. Although a sp potential is introduced as an auxiliary quantity, its choice conditions the rate of convergence of the expansion for the binding energy. Studies reported in Ref. [5] lead to conclude that the continuous choice for the auxiliary potential yields better convergence over the so called *standard choice*, where the sp potential is set to zero above the Fermi energy. Thus, we base this work on the continuous choice for the sp potentials.

This article is organized as follows. In Sec. 2 we layout the theoretical framework upon which we base the study of homogeneous nuclear matter at zero temperature. In Sec. 3 we present results for symmetric nuclear matter as well as neutronic matter, discuss associated effective masses and occurring *in-medium* di-nucleon structures. Additionally, we discuss extent to which Hugenholtz-van Hove theorem [9] for sp energies is met. In Sec. 4 we present a summary and the main conclusions of this work.

2 Framework

In BBG theory for homogeneous nuclear matter the g matrix depends on the density of the medium, characterized by the Fermi momentum k_F , and a starting energy ω . To lowest order in the BHF approximation for nuclear matter in normal state, when only two-body correlations are taken into account, the Brueckner G matrix satisfies

$$G(\omega) = v + v \frac{Q}{\omega + i\eta - \hat{h}_1 - \hat{h}_2} G(\omega), \quad (1)$$

with v the bare interaction between nucleons, \hat{h}_i the sp energy of nucleon i ($i = 1, 2$), and Q the Pauli blocking operator which for nuclear matter in normal state takes the form

$$Q|\mathbf{p}\mathbf{k}\rangle = \Theta(p - k_F)\Theta(k - k_F)|\mathbf{p}\mathbf{k}\rangle.$$

The solution to Eq. (1) enables the evaluation of the mass operator

$$M(k; E) = \sum_{|\mathbf{p}| \leq k_F} \langle \frac{1}{2}(\mathbf{k} - \mathbf{p}) | g_{\mathbf{K}}(E + e_p) | \frac{1}{2}(\mathbf{k} - \mathbf{p}) \rangle, \quad (2)$$

where the g matrix relates to G through

$$\langle \mathbf{k}'\mathbf{p}' | G(\omega) | \mathbf{k}\mathbf{p} \rangle = \delta(\mathbf{K}' - \mathbf{K}) \langle \frac{1}{2}(\mathbf{k}' - \mathbf{p}') | g_{\mathbf{K}}(\omega) | \frac{1}{2}(\mathbf{k} - \mathbf{p}) \rangle. \quad (3)$$

Here \mathbf{K} (\mathbf{K}') denotes the total momentum of the NN pair before (after) interaction, with $\mathbf{K} = \mathbf{k} + \mathbf{p}$, and $\mathbf{K}' =$

$\mathbf{k}' + \mathbf{p}'$, so that the Dirac delta functions expresses the momentum conservation. The sp energy becomes defined in terms of an auxiliary field U ,

$$e(p) = \frac{p^2}{2m} + U(p), \quad (4)$$

with m the nucleon mass taken as the average of proton and neutron masses. In the BHF approximation the sp potential is given by the on-shell mass operator,

$$U(k) = \text{Re } M[k; e(k)], \quad (5)$$

self-consistency requirement which can be achieved iteratively. We have used the continuous choice for the sp fields, so that this condition is imposed at all momenta k [10].

3 Results

We have proceeded to obtain self-consistent solutions for the sp fields $U(k)$ in infinite nuclear matter at various densities, specified by Fermi momenta $k_F \lesssim 2.5 \text{ fm}^{-1}$. These searches comprise isospin-symmetric nuclear matter and pure neutron matter. The internucleon interactions considered in this study are AV18 [8], Paris [11], Nijmegen I and II bare potentials [12]. In addition to these potentials we include a chiral effective-field-theory (χ EFT) interaction based on chiral perturbation theory. The resulting bare interaction is constructed with nucleons and pions as degrees of freedom, with the two-nucleon (2N) part fit to NN data. We consider the chiral 2N force (2NF) up to next-to-next-to-next-to-leading order (N^3 LO) given by Entem and Machleidt [2]. We also consider chiral 3N forces (3NF) in N^2 LO, using a density-dependent 2NF at the two-body level [13,14]. This density-dependent contribution does not contain correlation effects [15], and is added to the bare 2NF in the calculation of the G matrix. The corresponding Hartree-Fock contribution is subtracted at each iteration to avoid any double counting. For this chiral 3NF contribution, we use the low energy constants $c_D = -1.11$ and $c_E = -0.66$, reported in Ref. [16], which describe the ^3H and ^4He binding energies with unevaluated NN interactions.

All applications include partial waves up to $J = 7$ in the NN total angular momentum. For the numerical methodology to treat di-nucleons during self-consistency search we refer the reader to Ref. [7]. Files containing self-consistent solutions for sp potentials can be retrieved from Ref. [17].

3.1 Symmetric nuclear matter

The study of SNM requires to take into account NN states with total isospin $T = 0$, and $T = 1$. As a result, one has to include the attractive $^3\text{SD}_1$, $^3\text{PF}_2$ and $^1\text{S}_0$ channels. As reported in Ref. [7], the calculation of the on-shell mass operator to obtain $U(k)$ requires the evaluation of $g_{\mathbf{K}}(\omega)$ at various configurations of total momentum K of the NN

pair and starting energy $\omega = e(p) + e(k)$. In the process the g matrix is sampled over regions where it becomes singular, near or at the occurrence of *in-medium* bound states in these channels. This feature, investigated in the context of AV18 interaction, has led to unveil coexisting sp solutions at Fermi momenta slightly below 0.3 fm^{-1} , that is to say different solutions that meet self-consistency at the same k_F . Details about how these coexisting solutions are disclosed are given in the same reference. In this work we proceed in the same way.

Once a sp solution $U(k)$ is obtained for a given Fermi momentum we can evaluate the energy per nucleon E/A , which in the case of two-body forces is given by

$$\frac{E_{2N}}{A} = \frac{\sum_k n(k) \left[\frac{k^2}{2m} + \frac{1}{2}U(k) \right]}{\sum_k n(k)}. \quad (6)$$

In this work we use $n(k) = \Theta(k_F - k)$, i.e. nuclear matter in normal state. When 3NFs are included in BHF calculations, these enter at two levels. First, a density-dependent effective two-body interaction is added to the bare 2NF in a standard G -matrix calculation. In addition, the total energy has to be corrected to avoid double counting of the 3NF contribution [14, 18]. At the lowest order this can be achieved by subtracting the Hartree-Fock contribution due to 3NFs only:

$$\frac{E_{3N}}{A} = \frac{E_{2N}}{A} - \frac{1}{12} \frac{3}{k_F^3} \int_0^{k_F} k^2 dk \Sigma_{HF}^{3NF}(k). \quad (7)$$

We stress that the Hartree-Fock self-energy Σ_{HF}^{3NF} coming from the 3N force is calculated from an effective 2N potential at the lowest order, in keeping with the procedure established Ref. [14].

In Fig. 1 we present results for the energy per nucleon E/A as function of k_F for symmetric nuclear matter. Here, solid, long-, medium- and short-dashed curves denote AV18, Paris, Nijmegen I and II solutions, respectively. Dotted and dash-dotted curves represent solutions based on $N^3\text{LO}$ and $N^3\text{LO}+3\text{N}$ chiral interactions, respectively. Labels I and II are used to distinguish the two families of solutions. We are aware that, from a physical point of view, the energy of the system should be uni-valuated. The purpose of this figure in displaying separately E/A for the two phases is that of providing a global characterization of the sp solutions. An actual evaluation of the energy of the system at a given k_F would require a more comprehensive analysis, considering contributions from di-nucleons in the different channels and competing phases I and II. Under such considerations the scope of the BHF approximation would become limited.

The results presented in Fig. 1 show that all interactions considered yield nearly identical behavior in the range $0 \leq k_F \leq 0.4 \text{ fm}^{-1}$. Additionally, they all exhibit coexisting sp solutions at k_F in the range between ~ 0.13 and $0.28 - 0.30 \text{ fm}^{-1}$. In this regard the feature of coexistence is robust under the bare internucleon bare interaction.

In Fig. 2 we present results for the energy per nucleon E/A in SNM as a function of k_F for solutions in

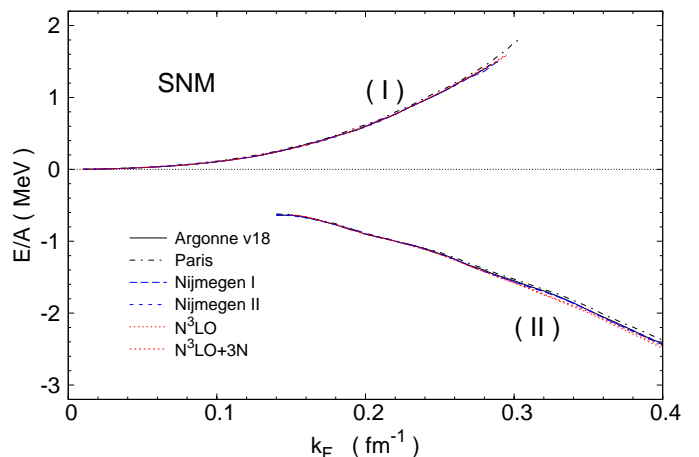


Fig. 1. Energy per nucleon for isospin-symmetric nuclear matter as function of Fermi momentum k_F . Solid, long-, medium- and short-dashed curves correspond to AV18, Paris, Nijmegen I and II, respectively. Dotted and dash-dotted curves represent solutions for $N^3\text{LO}$ and $N^3\text{LO}+3\text{N}$ chiral interactions, respectively.

phase II. We use the same convention of curve patterns as in Fig. 1. In this case the interactions exhibit different behaviors, resulting in different saturation points. As observed, chiral interactions are the ones which yield extreme values for the density and binding energy at saturation. On the one side $N^3\text{LO}$ saturates at $k_F = 1.85 \text{ fm}^{-1}$, with $E/A = -25.7 \text{ MeV}$, whereas $N^3\text{LO}+3\text{N}$ does so at $k_F = 1.30 \text{ fm}^{-1}$, with $E/A = -12.1 \text{ MeV}$. The former becomes much too bound at a density $\sim 2.7\rho_0$, with $\rho_0 = 0.16 \text{ fm}^{-3}$, the accepted saturation density. The latter, instead, saturates near the correct density but becomes underbound by $\sim 4 \text{ MeV}$ relative to the accepted value of $16 \pm 1 \text{ MeV}$. These results are comparable to those reported in Ref. [15]. Furthermore, at k_F below $\sim 1 \text{ fm}^{-1}$, i.e. matter density below 0.07 fm^{-3} , the behavior of E/A appears insensitive to the interaction. This feature is in agreement with recent reports based on BHF and Monte Carlo calculations using chiral interactions [19, 20].

Another feature we note from Fig. 2 is the similarity between AV18 and Paris potentials in their E/A vs k_F behavior. Their resulting saturation energies are -16.8 and -16.3 MeV , respectively, with both interactions saturating at a density near $1.4\rho_0$. In the cases of Nijmegen I and II saturation occurs at $2\rho_0$ and $1.8\rho_0$, respectively, while their respective binding occur at -20.6 and -18.3 MeV .

The results we provide here are in reasonable agreement with those reported elsewhere [21]. What is new in these results is the actual account for di-nucleon singularities in the g matrix to obtain self-consistent sp fields within BHF. Unfortunately there is now way to artificially suppress di-nucleon occurrences, without altering the bare interaction, in order to isolate the role of *in-medium* bound states.

The study of nucleon effective masses m^* has been subject of interest in various sub-fields [22, 23]. The calculated sp spectra of Eq. (4) allows us to evaluate the

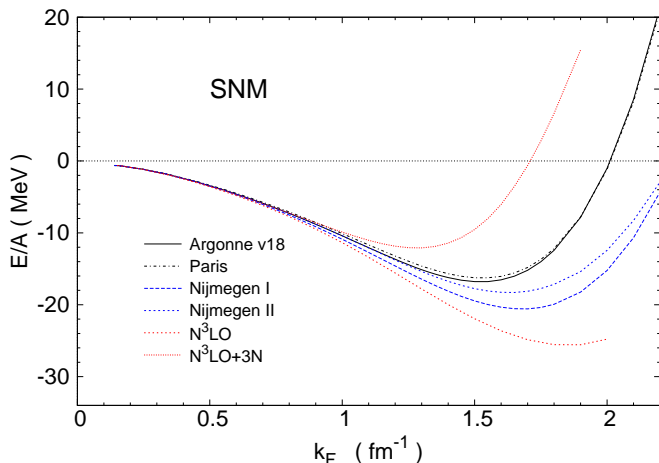


Fig. 2. Energy per nucleon for isospin-symmetric nuclear matter as function of Fermi momentum k_F . Curves follow the same convention as in Fig. 1.

effective mass

$$\frac{m^*}{m} = \frac{k_F}{m} \left[\frac{\partial \epsilon(k)}{\partial k} \right]_{k=k_F}^{-1}, \quad (8)$$

with m the nucleon mass. In Fig. 3 we plot the calculated effective-to-bare mass ratio m^*/m as a function of Fermi momentum based on the six interactions we have discussed. Filled and empty circles correspond to results for AV18 and Paris potentials, respectively. Filled and empty squares correspond to Nijmegen I and II potentials, respectively. Filled and empty diamonds denote solutions based on N^3LO and N^3LO+3N chiral interactions, respectively. Labels I and II refer to solutions in phase I and II, respectively.

A peculiar feature observed in Fig. 3 is the occurrence of $m^*/m > 1$ at Fermi momenta below $\sim 1 \text{ fm}^{-1}$. In the case of phase I, which starts at $k_F = 0$, the effective mass grows from the bare mass m up to $\sim 4m$ near the maximum k_F of phase I, consistent with findings reported in Ref. [7]. We also note that the trend followed by m^*/m vs k_F is very similar for all the interactions considered, an indication of the robustness of the results under changes of the bare internucleon potential. In the case of phase II, the range where $m^* > m$ is restricted to $\sim 0.2 < k_F \lesssim 1.1 \text{ fm}^{-1}$, or equivalently $\sim 0.003 < \rho/\rho_0 \lesssim 0.6$. As discussed in Refs. [7,24], this feature is closely related to the occurrence of di-nucleon bound states. For k_F near normal densities, i.e. in the range $1.4 - 1.5 \text{ fm}^{-1}$, the ratio m^*/m lies within the interval $0.78 - 0.85$ for all interactions, feature consistent with the typical values of nucleon effective masses.

3.2 Pure neutron matter

The case of pure neutron matter features full suppression of the deuteron channel. Therefore, singularities of

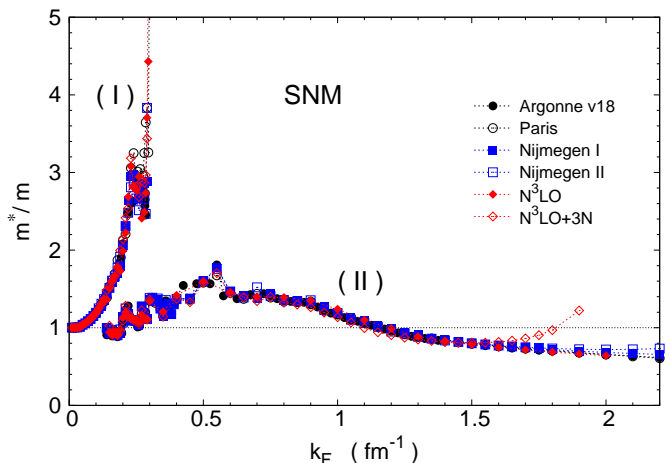


Fig. 3. Nucleon effective mass in isospin-symmetric nuclear matter as function of Fermi momentum k_F . Filled and empty circles represent solution for AV18 and Paris potentials, respectively. Filled and empty squares correspond to Nijmegen I and II potentials, respectively. Filled and empty diamonds denote solutions based on N^3LO and N^3LO+3N chiral interactions, respectively. Dotted lines are used to guide the eye.

$g_K(\omega)$ represent *in-medium* bound states formed by neutron pairs, i.e. di-neutrons. The treatment of these singularities is the same as that applied in SNM reported in Ref. [7]. In contrast to the case of SNM, however, no coexisting sp spectra are found.

In Fig. 4 we present results for the energy per nucleon, E/A , for neutronic matter as a function of k_F . We use the same convention of curve patterns as in Fig. 1. As observed, all interactions yield nearly identical energy per nucleon up to $k_F \sim 1 \text{ fm}^{-1}$, departing from each other at Fermi momenta above 1.2 fm^{-1} . All interactions yield monotonic growing E/A as function of k_F , with N^3LO+3N providing the highest slope. As in the case of SNM, AV18 and Paris potentials behave very similarly. The smallest slope in the energy comes from N^3LO , although both Nijmegen I and II present similar density dependence. For k_F below $\sim 1.2 \text{ fm}^{-1}$, i.e. neutron densities below 0.06 fm^{-3} , all interactions exhibit nearly the same behavior, in agreement with other reports based on chiral interactions [19,20].

Effective masses associated to the sp fields for pure neutron matter are shown in Fig. 5. Here we consider all six interactions included in the previous analysis, following the same symbol convention as in Fig. 3. As in the case of SNM, all interaction follow a very similar behavior as function of k_F , with only the chiral interaction N^3LO+3N departing from the rest at k_F above 1.5 fm^{-1} . It is also clear that the neutron effective mass is greater than its bare mass at k_F in the range $0.04 - 1.1 \text{ fm}^{-1}$, with a maximum value of $\sim 1.2m$ at k_F in the range $0.25 - 0.5 \text{ fm}^{-1}$. In the case of N^3LO+3N interaction the ratio m^*/m exhibits a growth at k_F above 1.5 fm^{-1} , which could be attributed to the relevance of the (density-dependent) $3N$ force at such high densities. Apart from this interaction at high densities, the behavior of effective masses featuring

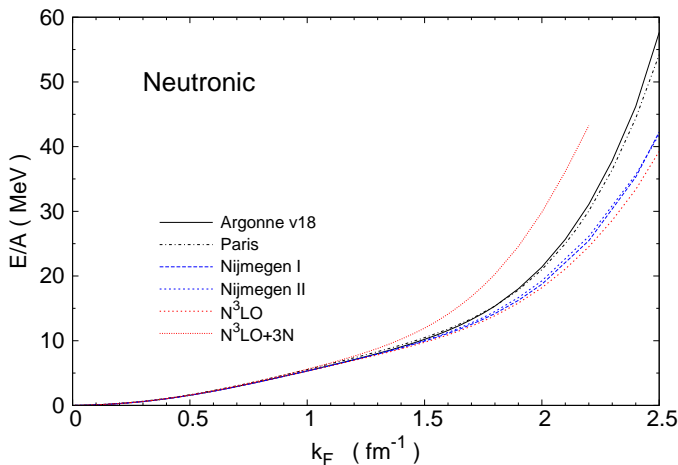


Fig. 4. Energy per nucleon for pure neutron matter as function of Fermi momentum k_F . Curves follow the same convention as in Fig. 1.

$m^*/m > 1$ is also robust under the choice of bare interaction being considered.

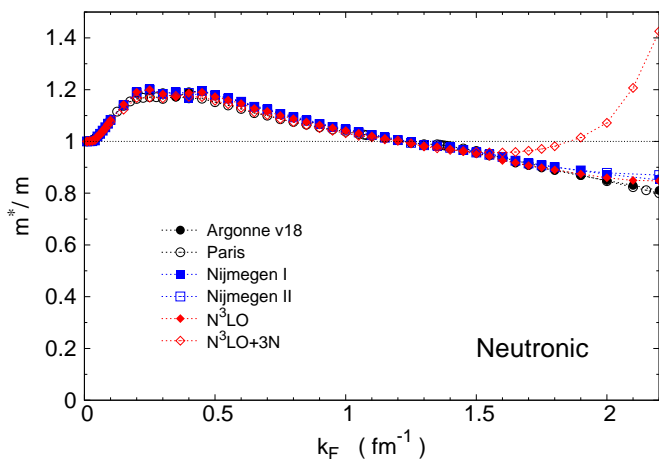


Fig. 5. Neutron effective mass in pure neutron matter as function of Fermi momentum k_F . Symbols follow the same convention as in Fig. 3.

3.3 Di-nucleons within BHF

As mentioned above, the occurrence of singularities in the g matrix denotes the presence of bound states. This feature becomes explicit with the use of the Lehmann spectral representation for the g matrix [3]

$$g_K(\omega) = v + \sum_{\alpha} v \frac{|\alpha\rangle\langle\alpha|}{\omega + i\eta - \epsilon_{\alpha}} Qv, \quad (9)$$

where α runs over discrete and continuous states, $|\alpha\rangle$ is an eigenstate of the Hamiltonian $\hat{H} = \hat{h}_1 + \hat{h}_2 + v$, with

eigenenergy ϵ_{α} . The way to infer the energy of bound states for a given pair momentum K is by imposing [7]

$$\det[1 - v\Lambda_K(\omega)] = 0, \quad (10)$$

with $\Lambda_K(\omega) = Q/(\omega - \hat{h}_1 - \hat{h}_2)$, the BHF particle-particle propagator. The energy of the bound state is obtained from the difference

$$b \equiv \omega - \omega_{th}, \quad (11)$$

where ω_{th} corresponds to the lowest (threshold) particle-particle energy allowed by the Pauli blocking operator.

We investigate the occurrence of di-nucleon bound states in SNM in the channels ${}^3\text{SD}_1$ and ${}^1\text{S}_0$ as a function of the Fermi momentum for all six NN interactions under study. The condition given by Eq. 10 can be investigated for selected values of K , the momentum of the NN pair. In the following we focus on center-of-mass at rest ($K = 0$). Fig. 6 shows results obtained for the di-nucleons in the deuteron channel, where we follow the same symbol convention as in Fig. 3. Labels I and II indicate solutions for phase I and II, respectively. From these results we observe bound states in channel ${}^3\text{SD}_1$ take place in phase I at momenta over the range $0 \leq k_F \lesssim 0.3 \text{ fm}^{-1}$, featuring increasing binding. The highest binding takes place at the upper edge of phase I, where $b \approx -4.5 \text{ MeV}$, nearly twice the binding energy of the deuteron in free space. It is also clear that all six interactions yield nearly the same binding. Phase II, in turn, shows bound states from $k_F \approx 0.14 \text{ fm}^{-1}$ up to k_F between 1.3 and 1.4 fm^{-1} , close to the accepted Fermi momentum at saturation. The maximum binding takes place at $k_F \approx 0.5 \text{ fm}^{-1}$, where $b \approx -2.6 \text{ MeV}$. Overall, all interactions display the same behavior for b .

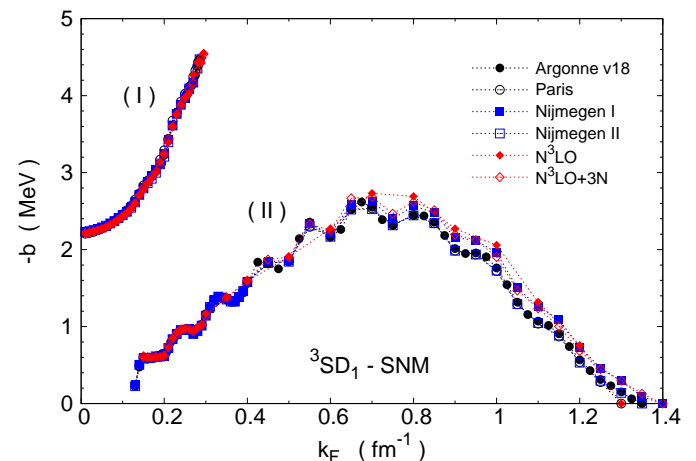


Fig. 6. *In-medium* deuteron binding energy in isospin-symmetric nuclear matter as function of the Fermi momentum k_F . Symbols follow the same convention as in Fig. 3.

Results for the ${}^1\text{S}_0$ channel in SNM are shown in Fig. 7 using the same notation as in the previous figure. Note that in this case the energy scale is expressed in keV units.

As a result, differences in the binding energy from the different NN interactions appear enhanced. With the exception of Paris potential (open circles), the trend followed by b in phase I is quite similar among the other five interactions, leading to a maximum binding of about 600 keV at $k_F \approx 0.28 \text{ fm}^{-1}$. Note also that for k_F below $\sim 0.06 \text{ fm}^{-1}$ no di-nucleon bound states take place, feature shown by all six interactions. This is consistent with the fact that no bound state takes place at zero density (free space) in the 1S_0 channel. In the case of phase II, di-nucleons take place from $k_F \gtrsim 0.2 \text{ fm}^{-1}$ up to about k_F slightly above 1 fm^{-1} . The maximum binding takes place at $k_F \approx 0.7 \text{ fm}^{-1}$, with b in the range 500 – 650 keV.

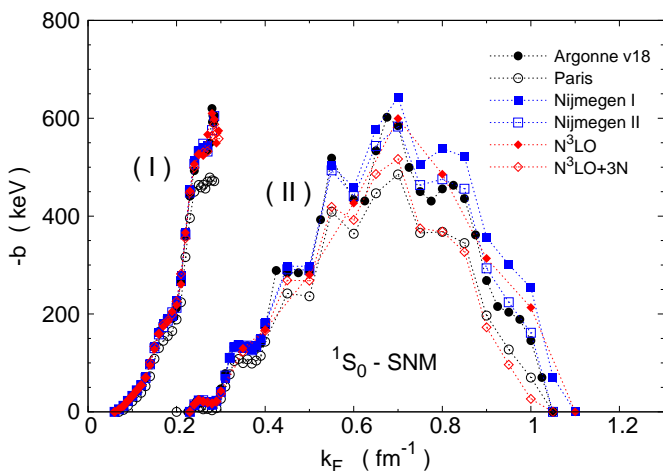


Fig. 7. *In-medium* di-nucleon binding energy in channel 1S_0 for isospin-symmetric nuclear matter as functions of the Fermi momentum k_F . Symbols follow the same convention as in Fig. 3.

Results for di-neutrons in pure neutron matter are shown in Fig. 8, where we plot b_{nn} as a function of k_F considering all six interactions in this study, applying the same notation as in the previous case. Here we also use keV units for the energy scale. Note that all interactions display similar behavior over k_F , with appearance of di-neutrons at k_F above 0.06 fm^{-1} and disappearance at $k_F \approx 1.05 \text{ fm}^{-1}$ in the case of Paris and $N^3\text{LO}+3\text{N}$ interactions, and at $k_F \approx 1.1 \text{ fm}^{-1}$ for the rest. The maximum binding takes place in the vicinity of $k_F \approx 0.6 \text{ fm}^{-1}$, with Paris potential leading to the lowest binding of $\sim -550 \text{ MeV}$. Note that the behavior of b_{nn} in this case shows some quantitative resemblance to that found for the 1S_0 channel in SNM (c.f. Fig. 7).

3.4 Hugenholtz-van Hove theorem

The Hugenholtz-van Hove (HvH) theorem [9] states a very general result that relates the mean energy of a bound system, E/N , with its chemical potential μ . At zero temperature this relationship establishes that [1]

$$p = -\frac{E}{V} + \frac{N}{V}\mu, \quad (12)$$

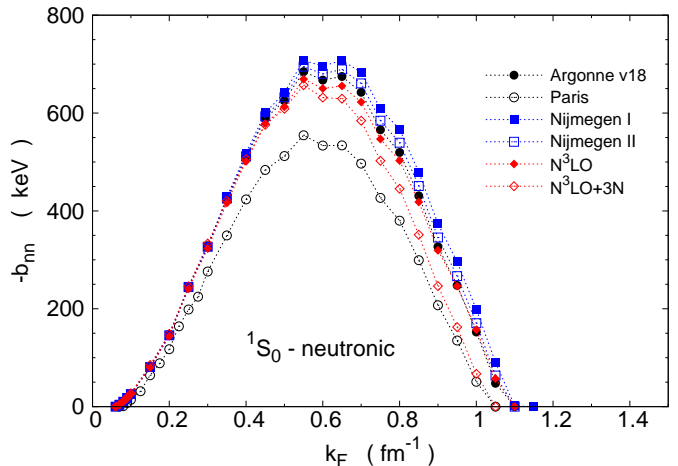


Fig. 8. *In-medium* di-neutron binding energy in pure neutron matter as function of the Fermi momentum k_F . Symbols follow the same convention as in Fig. 3.

where p represents the pressure, E/V the energy density, N/V the particle density, and μ the chemical potential. The latter should be extracted from the derivative of energy with respect to the number of particles. In the BHF approximation at zero temperature the chemical potential coincides with the Fermi energy e_F of the system –given by the sp energy at the Fermi momentum k_F – hence relying on the auxiliary potential $U(k)$. Since at saturation the pressure vanishes, Eq. (12) reduces to

$$\frac{E}{A} = e_F, \quad (13)$$

with A the nucleon number. It has been known for some time that the HvH theorem is not satisfied in the BHF approximation for nuclear matter at zero temperature. This limitation has led to go beyond BHF by including higher order contributions in the hole expansion for the nucleon self-energy [25,26,27]. Such an extension goes beyond the scope of this work. However, it is still instructive to assess the extent to which HvH theorem is violated within the BHF approach for the interactions considered in this work.

In Table 1 we list the internucleon potentials together with their respective Fermi momentum and density ρ at saturation. The sixth column displays the difference between the mean energy E/A and the Fermi energy, $e_F = e(k_F)$. If HvH was satisfied at the saturation point, then Eq. 13 would imply only zeros for this column. Such is not the case, as we observe that the difference $(E/A - e_F)$ is comparable to $-E/A$. The weakest violation of HvH theorem occurs for $N^3\text{LO}+3\text{N}$ chiral interaction, where $E/A - e_F = 8.2 \text{ MeV}$.

The inclusion of higher-order correlations to mitigate the violation of the HvH theorem has been investigated in Refs. [25,26,27]. In the present context, this extension would require a significant amount of work. Implications of these considerations in actual calculations remain to be seen, particularly regarding the coexistence of sp solutions in the case of SNM.

Table 1. HvH theorem check at saturation point

Potential	k_F [fm ⁻¹]	ρ [fm ⁻³]	$\frac{E}{A}$ [MeV]	e_F [MeV]	$\frac{E}{A} - e_F$ [MeV]
AV18	1.52	0.237	-16.8	-34.5	17.7
Paris	1.53	0.242	-16.3	-33.7	17.4
Nijmegen I	1.68	0.320	-20.6	-40.5	19.9
Nijmegen II	1.63	0.293	-18.3	-36.8	18.5
N ³ LO	1.85	0.428	-25.7	-45.9	20.2
N ³ LO+3N	1.30	0.148	-12.1	-20.3	8.2

4 Summary and conclusions

We have investigated the role of di-nucleon bound states in homogeneous nuclear matter in the cases of isospin-symmetric matter and pure neutron matter. The study has been based on the BHF approach at zero temperature, considering modern bare internucleon interactions, including the case of 3NFs based on chiral N³LO with three-nucleon forces up to N²LO. Special attention is paid to the occurrence of di-nucleon bound states structures in the ¹S₀ and ³SD₁ channels, whose explicit treatment is critical for the stability of self-consistent solutions at sub-saturation densities. An analysis of these solutions is made by comparing their associated energy per nucleon E/A , effective masses and *in-medium* di-nucleon binding energies.

An important result from this work is that coexistence of sp solutions in SNM withing the BHF approximation, occurring at Fermi momenta in the range 0.13 – 0.3 fm⁻¹ and reported in Ref. [7], is a robust property of the system which does not depend on the choice of realistic internucleon potentials. Additionally, all interactions yield very similar behavior of E/A at fermi momenta $k_F \lesssim$ fm⁻¹. At higher densities the interactions exhibit their differences, resulting in different saturation points in the case of SNM, or different growth of E/A (i.e. pressure) as function of the density. Additionally, we also obtain effective masses larger than bare masses at sub-saturation densities, feature shared by all interactions. In the case of SNM, effective masses in phase I can reach up to four times the bare mass, while in the case of phase II a maximum ratio of $m^*/m \approx 1.5$ is found at $k_F \approx 0.5$ fm⁻¹. In the case of pure neutron matter, the highest effective masses occur in the range $0.25 \lesssim k_F \lesssim 0.5$ fm⁻¹, where m^*/m can reach up to ~ 1.2 .

Di-nucleons have also been investigated in both SNM and neutronic matter, identified from singularities in the g matrix at starting energies below particle-particle threshold energy. In this work we obtain results consistent to those reported in Ref. [7], but not restricted anymore to AV18 in SNM. Bound states are identified at sub-saturation densities, with deuterons in phase I bound at energies nearly twice that in free space. Deuterons in phase II reach maximum binding at $k_F \approx 0.7$ fm⁻¹, with binding energies comparable to that in free space. These *in-medium* bound states get dissolved for $k_F \gtrsim 1.3$ fm⁻¹, for all the interactions considered. Di-nucleons in channel ¹S₀ are found in

both, SNM and neutronic matter. Their binding is much weaker to that for deuterons, reaching deepest values between -700 and -500 keV. In this particular channel di-nucleons get dissolved at Fermi momenta above 1.1 MeV, feature shared by all interactions considered. Overall, the binding properties of di-nucleons appear quite comparable, pointing also to their robustness under the interaction being considered.

The occurrence of di-nucleons in nuclear matter is closely related to nuclear pairing phenomena, mechanism responsible for the formation of Cooper pairs and the emergence of superfluid and superconducting states of matter [28, 29]. This aspect, addressed to some extent in Ref. [7], has been omitted here since there would be no substantial new information. On this regard we have checked that all interactions behave very similar to AV18 potential. At a more basic level, in this work we have investigated the degree of fulfillment of Hugenholtz-van Hove theorem, finding that BHF approach alone fails considerably. However, studies reported in Refs. [25, 26, 27]. point that inclusion of higher order terms in the series expansion would remedy this limitation. Efforts to include rearrangement corrections are underway.

F.I. thanks CONICYT fellowship Beca Nacional, Contract No. 221320081. This work was supported in part by STFC through Grants ST/I005528/1, ST/J005743/1 and ST/L005816/1. Partial support comes from “NewCompStar”, COST Action MP1304.

References

1. M. Baldo, ed., *Nuclear Methods and the Nuclear Equation of State*, Vol. 8 of *International Review of Nuclear Physics* (World Scientific, Singapore, 1999).
2. D.R. Entem, R. Machleidt, *Phys. Rev. C* **68**, 041001 (2003).
3. W.H. Dickhoff, D. Van Neck, *Many-Body Theory Exposed* (World Scientific, Singapore, 2008).
4. Y. Dewulf, W.H. Dickhoff, D. Van Neck, E.R. Stoddard, M. Waroquier, *Phys. Rev. Lett.* **90**, 152501 (2003).
5. H.Q. Song, M. Baldo, G. Giansiracusa, U. Lombardo, *Phys. Rev. Lett.* **81**, 1584 (1998).
6. K. Amos, P.J. Dortmans, H.V. von Geramb, S. Karataglidis, J. Raynal, *Advances in Nuclear Physics*, Vol. 25 of *Advances in Nuclear Physics* (Springer, New York, 2000).
7. H.F. Arellano, J.P. Delaroche, *Eur. Phys. Journal A* **51**, 1 (2015).
8. R.B. Wiringa, V.G.J. Stoks, R. Schiavilla, *Phys. Rev. C* **51**, 38 (1995).
9. N.M. Hugenholtz, L. van Hove, *Physica* **24**, 363 (1958).
10. M. Baldo, A. Fiasconaro, *Phys. Lett. B* **491**, 240 (2000).
11. M. Lacombe, B. Loiseau, J.M. Richard, R.V. Mau, J. Côté, P. Pirès, R. de Tournell, *Phys. Rev. C* **21**, 861 (1980).
12. V.G.J. Stoks, R.A.M. Klomp, C.P.F. Terheggen, J.J. de Swart, *Phys. Rev. C* **49**, 2950 (1994).
13. J.W. Holt, N. Kaiser, W. Weise, *Phys. Rev. C* **81**, 024002 (2010).
14. K. Hebeler, A. Schwenk, *Phys. Rev. C* **82**, 014314 (2010).

15. A. Carbone, A. Rios, A. Polls, Phys. Rev. C **90**, 054322 (2014).
16. A. Nogga, P. Navrátil, B.R. Barrett, J.P. Vary, Phys. Rev. C **73**, 064002 (2006).
17. H.F. Arellano, *omp-online website* (2006), $U(k; k_F)$ solutions accessible for download, <http://www.omp-online.cl>.
18. A. Carbone, A. Polls, A. Rios, Phys. Rev. C **88**, 044302 (2013).
19. I. Tews, S. Gandolfi, A. Gezerlis, A. Schwenk, Phys. Rev. C **93**, 024305 (2016).
20. F. Sammarruca, L. Coraggio, J.W. Holt, N. Itaco, R. Machleidt, L.E. Marcucci, Phys. Rev. C **91**, 054311 (2015).
21. Z.H. Li, U. Lombardo, H.J. Schulze, W. Zuo, L.W. Chen, H.R. Ma, Phys. Rev. C **74**, 047304 (2006).
22. N. Chamel, Phys. Rev. Lett. **110**, 011101 (2013).
23. M. Baldo, G.F. Burgio, H.J. Schulze, G. Taranto, Phys. Rev. C **89**, 048801 (2014).
24. F. Isaule, H.F. Arellano, A. Rios, Phys. Rev. C **94**, 044317 (2016).
25. P. Czerski, A. De Pace, A. Molinari, Phys. Rev. C **65**, 044317 (2002).
26. W. Zuo, I. Bombaci, U. Lombardo, Phys. Rev. C **60**, 024605 (1999).
27. P. Grange, J. Cugnon, A. Lejeune, Nuclear Physics A **473**, 365 (1987).
28. R.A. Broglia, V. Zelevinsky, eds., *Fifty Years of Nuclear BCS* (World Scientific, Singapore, 2013).
29. A. Sedrakian, J.W. Clark, M. Alford, eds., *Pairing in Fermionic Systems* (World Scientific, Singapore, 2006).

